Nano Research 2018, 11(12): 6436–6446
https://doi.org/10.1007/s12274-018-2168-8
Research Article
ISSN 1998-0124
CN 11-5974/O4

Three-dimensional spongy framework as superlyophilic, strongly absorbing, and electrocatalytic polysulfide reservoir layer for high-rate and long-cycling lithium-sulfur batteries

Lianbo Ma[1,§], Guoyin Zhu[1,§], Wenjun Zhang[1], Peiyang Zhao[1], Yi Hu[1], Yanrong Wang[1], Lei Wang[1], Renpeng Chen[1], Tao Chen[1], Zuoxiu Tie[1], Jie Liu[1,2], and Zhong Jin[1] (✉)

[1] *Key Laboratory of Mesoscopic Chemistry of MOE, School of Chemistry and Chemical Engineering, Nanjing University, Nanjing 210023, China*
[2] *Department of Chemistry, Duke University, Durham, NC 27708, USA*
[§] *Lianbo Ma and Guoyin Zhu contributed equally to this work.*

Received: 13 June 2018
Revised: 25 July 2018
Accepted: 2 August 2018

KEYWORDS

lithium-sulfur batteries, composite spongy framework, polysulfide reservoir layer, chemisorption and absorbability, electrocatalytic effect

ABSTRACT

In the development of lithium-sulfur (Li-S) batteries, various approaches have been adopted to enhance the electronic conductivity of the sulfur cathode and alleviate the shuttle effect of polysulfides; however, the strategies providing efficient solutions are still limited. To further improve the electrochemical performance of Li-S batteries, in this work we propose a new strategy involving the incorporation of a three-dimensional functional spongy framework as polysulfide reservoir layer, with strong absorbability and electrocatalytic activity towards sulfur species. The spongy framework has a hierarchical architecture composed of highly conductive Ni foam/graphene/carbon nanotubes/MnO_2 nanoflakes (NGCM). The strongly interconnected Ni foam, graphene, and carbon nanotubes of the NGCM sponge facilitate electron transfer during discharge/charge processes; moreover, the superlyophilic properties of the NGCM sponge ensure good wettability and interface contact with the Li-S electrolyte, and the porous MnO_2 nanoflakes provide strong chemisorptive and electrocatalytic effects on polysulfides (as confirmed theoretically and experimentally). The NGCM sponge, serving as a polysulfide reservoir layer attached on a conventional sulfur-mixed carbon nanotubes (S/CNTs) cathode, can provide improved reversible capacity, rate capability (593 mAh·g^{-1} at 3.0 C), and cycling stability. In addition, the self-discharge rate is greatly reduced, owing to the efficient conservation of polysulfides in the NGCM spongy framework.

Address correspondence to zhongjin@nju.edu.cn

1 Introduction

Lithium-sulfur (Li-S) batteries with high theoretical capacity and high energy density have attracted considerable attention, because of the abundant nature and low cost of elemental sulfur [1–4]. Unfortunately, despite these obvious advantages, the practical application of Li-S batteries is still hindered by several problems, such as the low electronic conductivity and volume expansion of elemental sulfur [5–7], as well as the easy dissolution of long-chain polysulfides and the resulting shuttle effect [8, 9]. Various strategies have recently been investigated to address these issues, including the exploration of novel nanostructured sulfur hosts [10–24], the introduction of electrolyte additives [25, 26], and the protection of lithium anodes [27–29]. However, fully effective solutions that can simultaneously meet the high areal capacity and cycling stability requirements are still lacking.

In recent studies, owing to their structural advantages, nanostructured hybrid materials (N-doped graphene/carbon nanotubes (CNTs) [30], graphene/CNTs [31], and CNTs/SnO [32]) were employed as novel sulfur host materials, and the corresponding sulfur cathodes exhibited good performances. Herein, at variance with the above reports, we propose a novel strategy in which a three-dimensional (3D) porous spongy framework directly serves as an efficient polysulfide reservoir layer in Li-S batteries. The hybrid spongy framework is hierarchically assembled in a Ni foam/graphene sheets/CNTs/MnO_2 nanoflakes (NGCM) architecture, which provides a large contact area with the electrolyte. In this hierarchical spongy nanostructure, graphene sheets and entangled CNTs are uniformly grown on the surface of Ni foam, thereby allowing the homogeneous decoration with MnO_2 nanoflakes. The well-distributed hierarchical porous structure of Ni foam, graphene, and CNTs in the NGCM spongy framework allows the infiltration and conservation of the electrolyte, while the 3D-interconnected conductive network guarantees a smooth electron transfer. The layered MnO_2 nanostructure was selected to adsorb the polysulfides and catalyze their fast conversion, owing to its high contact area with the electrolyte, strong polysulfide chemisorption ability, and easy fabrication procedure through simple redox reactions between the carbon matrix and $KMnO_4$. With the assistance of the NGCM spongy framework as polysulfide reservoir layer, a conventional sulfur-mixed carbon nanotubes (S/CNTs)-based cathode exhibits highly improved electrochemical performance in terms of specific capacity, rate capability, and cycling stability, as well as a greatly reduced self-discharge rate.

2 Experimental details

2.1 Preparation of Ni foam/graphene/CNT (NGC) sponge

Typically, a piece of Ni foam (2 cm × 2 cm) was washed several times with 0.1 M HCl solution and absolute ethanol to remove possible surface contaminations and then pressed into a thin slice of ~ 0.3 mm thickness. The Ni foam was placed into a tube furnace for the growth of graphene, using ethanol vapor as carbon source and 120 sccm Ar/H_2 (4:1 in volume) as carrier gas. The growth temperature was set at 900 ℃ with a ramping rate of 10 ℃·min^{-1}. The as-prepared Ni foam/graphene (NG) was immersed in a 30 mL ethanol solution containing 0.2 M $Ni(NO_3)_2{\cdot}6H_2O$ and 100 mg of polyethylene glycol (PEG, M_W = 20,000, Aladdin) for 10 min, and then NGC was fabricated via another chemical vapor deposition (CVD) step at 700 ℃, with ethanol vapor as carbon source and 80 sccm Ar/H_2 (4:1 in volume) as carrier gas.

2.2 Preparation of NGCM sponge

Typically, 300 mg of PEG and 120 mg of $KMnO_4$ were dissolved in 30 mL of ethanol under ultrasonication. Then, this mixture and the above-prepared NGC were transferred and sealed in an autoclave. After heating at 70 ℃ for 4 h, the resulting product was washed several times with water to remove the impurities and vacuum-dried at 60 ℃ overnight.

2.3 Preparation of S/CNTs composite

Briefly, 30 mg of CNTs (TimesNano, Chengdu, China) and 70 mg of high-purity sulfur powder were mixed and ground in a mortar for 30 min. Then, the mixture was sealed in an autoclave and heated at 155 ℃ for 12 h.

After cooling down to room temperature naturally, the final product was collected.

2.4 Characterizations

Scanning electron microscopy (SEM) images, energy dispersive X-ray spectroscopy (EDX) profiles, and elemental mappings were collected on a FEI Nova NanoSEM-450 instrument. Transmission electron microscopy (TEM) measurements were performed on a JEOL JEM-2100F instrument using an accelerating voltage of 200 kV. The composition of the products was determined by elemental analysis (CHN-O-Rapid) and inductively coupled plasma-optical emission spectrometry (ICP-OES, Vista-MPX). Powder X-ray diffraction (XRD) patterns were recorded with a Bruker D-8 Advance diffractometer, using Cu Kα (λ = 1.5406 Å) radiation at a scanning rate of 6 °·min^{-1}. Raman analysis was performed on a Horiba JY Raman spectrometer using a 473 nm laser source. X-ray photoelectron spectroscopy (XPS) measurements were performed on a PHI-5000 VersaProbe spectrometer using Al Kα X-ray radiation. Contact angles were determined with a dynamic contact angle measuring device/tensiometer (OCA-30, DataPhysics Instruments GmbH). Nitrogen adsorption–desorption isotherms were obtained through Brunauer–Emmett–Teller (BET) analysis at 77 K on a Quantachrome Autosorb-IQ-2C-TCD-VP instrument. Thermogravimetric analysis (TGA) was performed on a Netzsch STA-449C instrument under N_2 atmosphere, from room temperature to 600 °C at a heating rate of 10 °C·min^{-1}.

2.5 Battery assembly and electrochemical measurements

The cathodes were prepared by mixing the S/CNTs composite, acetylene black, and the binder (polyvinylidene fluoride, PVDF) in N-methylpyrrolidinone (NMP) solvent, with weight ratios of 80:10:10. The mixture was stirred for 24 h, spread on an aluminum foil, and then dried in a vacuum oven at 60 °C to remove the solvent. Li-S coin cells were assembled in an argon-filled glovebox with the above-prepared S/CNTs composite cathode, a commercial Celgard separator, and a lithium foil anode. The diameter of the sulfur composite electrode was 10 mm, whereas the areal sulfur loading was approximately 1.3 mg·cm^{-2}. The electrolyte was 1.0 M bis(trifluoromethane)sulfonamide lithium (LiTFSI) dissolved in a 1,2-dimethoxyethane/1,3-dioxolane (DME/DOL, 1:1 in volume, with 1.0 wt.% $LiNO_3$ additive) solvent mixture. The electrolyte amount was approximately 8 μL per mg of sulfur loading mass. The NGCM or NGC sponge framework was sandwiched between the S/CNTs cathode and the separator as a polysulfide reservoir layer. Li-S coin cells without polysulfide reservoir layer were also prepared for comparison. The cycling stability of the Li-S cells was measured on a Land CT2001A analyzer under different current rates. Electrochemical impedance spectroscopy (EIS) measurements were carried out in the range of 100 kHz to 0.01 Hz.

2.6 Computational methods

The density functional theory (DFT) method was employed to calculate the binding energies (E_b) between the MnO_2 host and adsorbed sulfur species, defined by

$$E_{ads} = E_{s+host} - E_s - E_{host} \quad (1)$$

where E_{s+host}, E_s, and E_{host} are the energies of the sulfur species-host material, sulfur species, and host material, respectively. The initial conformation of all molecules was obtained by the molecular mechanics (MM) method (using the Forcite module of the Accelrys Materials Studio software). The DFT calculations were performed with the Dmol3 module of Accelrys Materials Studio. The exchange-correlation functional was approximated by the Perdew–Burke–Ernzerhof (PBE) method. DFT semicore pseudopotentials were used to calculate the core–electron interactions. The DFT-D (where D stands for dispersion) approach, with the Ortmann–Bechstedt–Schmidt (OBS) van der Waals (vdW) correction, was used to accurately describe the vdW interactions, which influence the adsorption configurations of sulfur species on the host material. Solvation effects were treated by the COSMO model, using a dielectric constant of 6.18 to mimic the mixed DME/DOL solvent.

3 Results and discussion

For the preparation of the NGCM spongy framework, graphene layers were first grown on the surface of

pressed/compacted Ni foam (forming NG) through CVD using ethanol as carbon source, as illustrated in Fig. 1(a). Subsequently, through a similar CVD step, intertwined CNTs were grown on the surface of NG with Ni species as catalyst and ethanol as carbon source, forming the NGC hierarchical structure. Finally, ultrathin MnO_2 nanoflakes were decorated around the CNTs via a conventional hydrothermal method under mild conditions. Notably, each component in the NGCM sponge architecture is interconnected with the others, thus enabling high structural integrity and electrical conductivity. Conventional Li-S batteries are known to suffer from the shuttle effect of dissolved polysulfides, which results in serious capacity deterioration, as illustrated in Fig. 1(b). By adopting the lyophilic NGCM spongy framework with 3D hierarchical porous structure as polysulfide uptake layer, the shuttle effect can be effectively suppressed through the strong chemisorption capability (Fig. 1(c)), as detailed below. Moreover, we found that the high electrocatalytic activity originating from the decorated MnO_2 nanoflakes can effectively promote the polysulfide redox reactions. Benefitting from these favorable features, Li-S batteries with the NGCM spongy framework were found to exhibit greatly enhanced electrochemical performance.

The morphological features of the samples were investigated by SEM. As the original porous framework, the pressed Ni foam shows a 3D macroporous structure and a smooth surface (Fig. S1 in the Electronic Supplementary Material (ESM)). After the growth of graphene, the 3D grid structure is well maintained with no structural collapse, and micron-size graphene domains are evenly coated on the surface (Figs. 2(a)–2(c)). The thickness of the graphene sheets wrapped around NG is around 1–5 layers, as evidenced by the TEM image in Fig. 2(d). The subsequent growth of CNTs on the surface of graphene sheets can provide a villous and hierarchical 3D

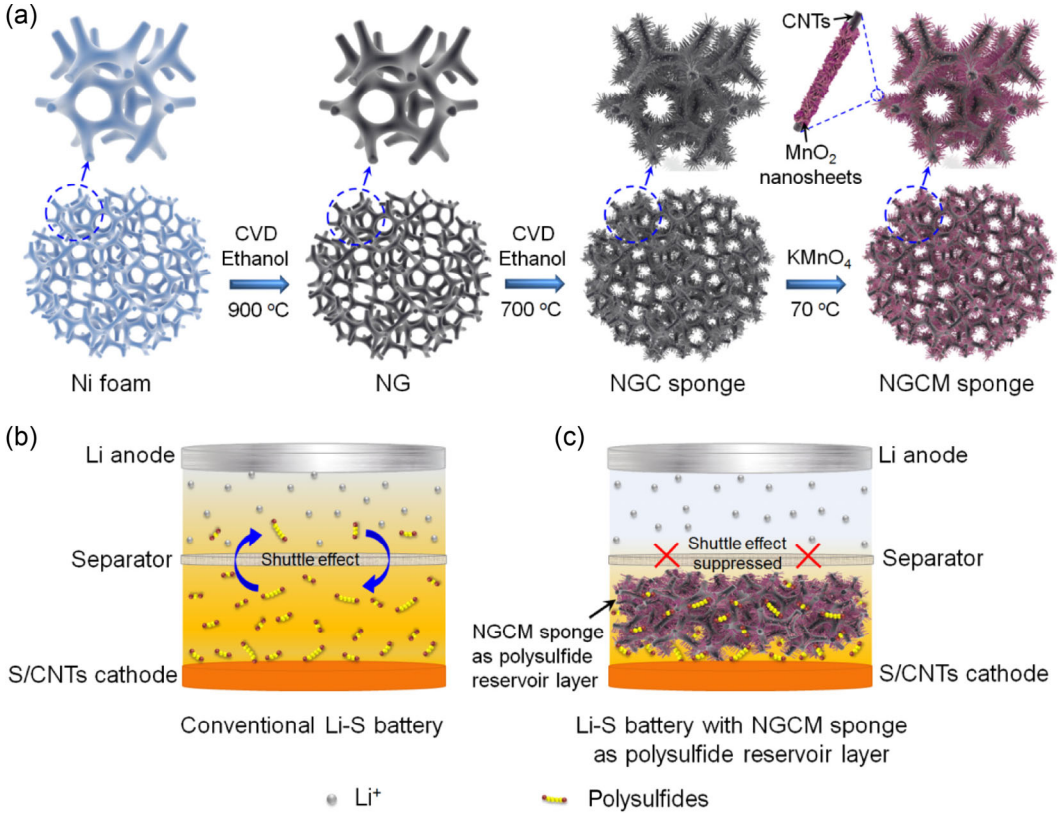

Figure 1 Synthesis of 3D NGCM spongy framework and corresponding functional mechanism in Li-S batteries. (a) Schematic illustration of the synthesis of the NGCM sponge. Schematic diagram of (b) conventional Li-S battery suffering from serious polysulfide shuttle effects and (c) Li-S battery with NGCM sponge as polysulfide reservoir layer for preventing the shuttle effect.

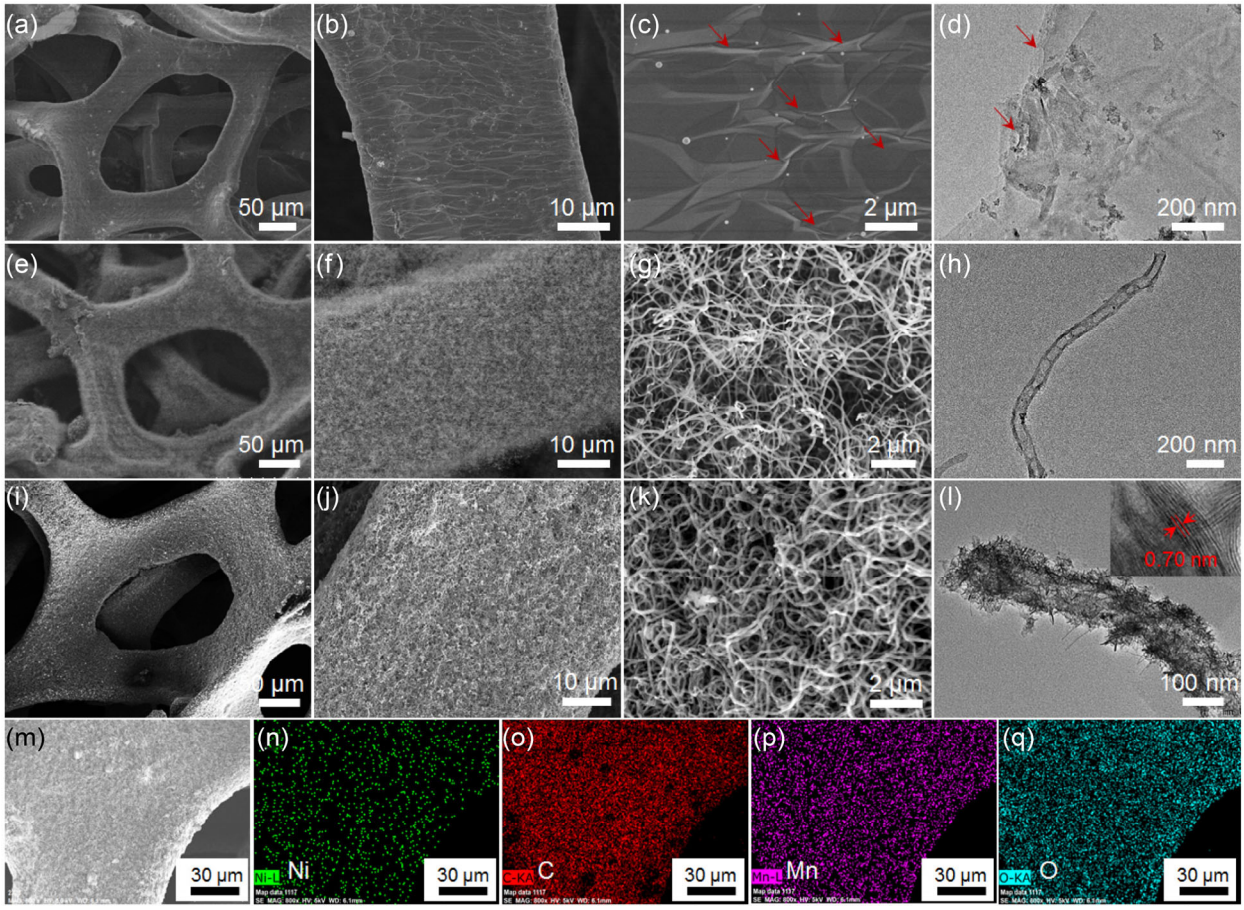

Figure 2 Morphological and compositional characterizations of the samples. (a)–(c) SEM images of NG and (d) TEM image of graphene sheets scraped from the surface of NG. (e)–(g) SEM images of NGC at different magnifications and (h) TEM image of an individual CNT grown on top of NGC. (i)–(k) SEM images of NGCM at different magnifications. (l) TEM image of an individual CNT decorated with ultrathin MnO_2 nanoflakes; the inset shows a high-resolution TEM (HRTEM) image of MnO_2 nanoflakes with a lattice distance of 0.70 nm. (m) SEM image of NGCM and (n)–(q) corresponding elemental mappings of Ni, C, Mn, and O.

structure coated with carbon, which is desirable for the decoration with MnO_2 nanoflakes, and thus very important for the overall structural design (Figs. 2(e)–2(g)). The randomly-oriented and densely-packed CNTs grown on NGC show an average diameter of ~ 70 nm (Fig. 2(h)) and a length of ~ 10 μm. After the loading of ultrathin MnO_2 nanoflakes, the final NGCM spongy framework fully inherited the 3D structure, while the diameter of CNTs/MnO_2 showed a clear increase due to the homogeneous coating of MnO_2 (Figs. 2(i)–2(k)). As shown by the TEM analysis, ultrathin MnO_2 nanoflakes with a thickness of several nanometers were vertically grown on the side walls of the CNTs (Fig. 2(l)). The observed lattice distance of 0.70 nm corresponds to the (110) plane of MnO_2. The EDX elemental mappings revealed the coexistence and homogeneous distribution of Ni, C, Mn, and O elements (Figs. 2(m)–2(q)). The elemental analysis and ICP-OES measurements reveal Ni, C, and Mn element contents of about 79.5 wt.%, 9.83 wt.%, and 6.73 wt.%, respectively.

The crystallinity of NGCM was investigated by XRD (Fig. S2 in the ESM) analysis, which revealed the characteristic peaks of metallic Ni, graphitic carbon, and MnO_2. The Raman spectrum of NG highlights the presence of few-layer graphene sheets (Fig. S3 in the ESM) [33, 34]. In the case of NGC, an additional Raman peak appears at ~ 1,355 cm^{-1}, originating from the D band of the CNTs. The Raman spectrum of NGCM displays a broad Raman band at ~ 590 cm^{-1}, corresponding to the Mn–O bonds in MnO_2 [35, 36]. The composition and chemical states of the NGCM

sponge were investigated by XPS (Fig. S4 in the ESM). The XPS spectrum of the Mn 2p region (Fig. S4(b) in the ESM) consists of two doublets at 653.9 eV (Mn $2p_{1/2}$) and 642.3 eV (Mn $2p_{3/2}$), whose binding energy difference (11.6 eV) indicates the formation of MnO_2 [37].

The surface areas and porosity of the as-prepared samples were investigated by N_2 adsorption–desorption isotherms (Figs. 3(a)–3(d)). The specific surface areas of Ni foam, NG, NGC, and NGCM spongy frameworks measured by the BET method were 0.21, 0.32, 14.5, and 87.5 $m^2 \cdot g^{-1}$, respectively, corresponding to areal surface areas of 0.009, 0.012, 0.75, and 11.3 $m^2 \cdot cm_{sponge}^{-2}$, respectively. This result demonstrates a significantly improved contact interface between NGCM sponge and Li-S electrolyte. The corresponding pore size distributions, displayed in Fig. S5 in the ESM, reveal the existence of mesopores. The wettabilities of the samples by the DOL/DME (1:1 in volume) solution were then compared. Interestingly, the contact angles of Ni foam, NG, NGC, and NGCM spongy frameworks with the DOL/DME solution were measured to be 17.3°, 8.2°, 0°, and 0°, respectively, as shown in Figs. 3(e)–3(h). Remarkably, the NGC and NGCM sponges show superlyophilicity for the DOL/DME solution, confirming their excellent wettability for the absorption and reservation of the Li-S electrolyte.

The enhancement effect of the NGCM sponge on the electrochemical performance of Li-S batteries based on the S/CNTs composite cathode (as detailed in the Experimental section and Figs. S6 and S7 in the ESM) was systematically verified. The NGCM spongy framework was sandwiched between the S/CNTs cathode and the separator as polysulfide reservoir layer. For comparison, Li-S cells with the NGC sponge (not decorated with MnO_2 nanoflakes) or without spongy framework were also assembled. The galvanostatic discharge/charge profiles at 0.2 C of S/CNTs cathode-based Li-S cells assembled with or without spongy framework are presented in Fig. 4(a). The Li-S cells with NGCM sponge layer show a typical two-plateau discharge behavior, corresponding to the two cathodic peaks in cyclic voltammetry (CV) curves [38]. The two discharge plateaus are related to the reduction of S_8 to higher-order polysulfides (Li_2S_x, $4 \le x < 8$) and the further formation of lower-order polysulfides (Li_2S_2 or Li_2S) [38–44]. The presence of only one charge plateau suggests the one-step oxidation of lower-order polysulfides to elemental sulfur [45]. Notably, the Li-S cells with the NGC sponge or without spongy layer exhibit lower discharge capacity and much larger potential polarizations compared to those with the NGCM sponge. These results indicate the strong electrocatalytic effect of the

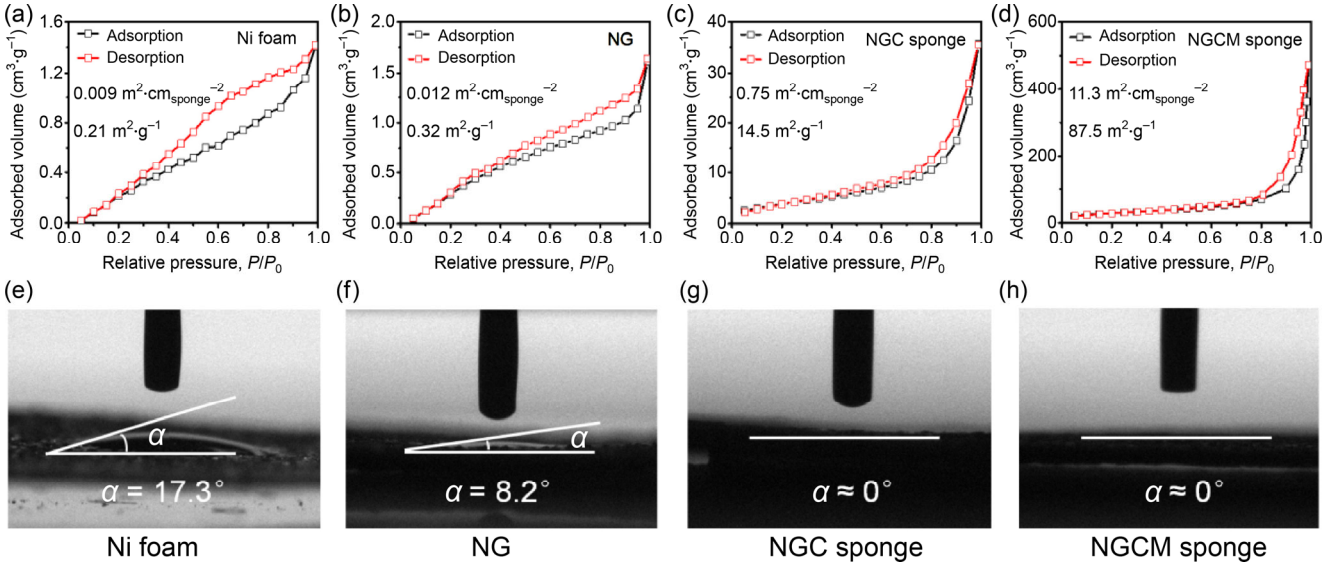

Figure 3 Surface area and wettability of spongy frameworks. (a)–(d) N_2 adsorption–desorption isotherms of (a) Ni foam, (b) NG, (c) NGC, and (d) NGCM spongy frameworks. (e)–(h) Contact angles of (e) Ni foam, (f) NG, (g) NGC, and (h) NGCM spongy frameworks with DOL/DME solution.

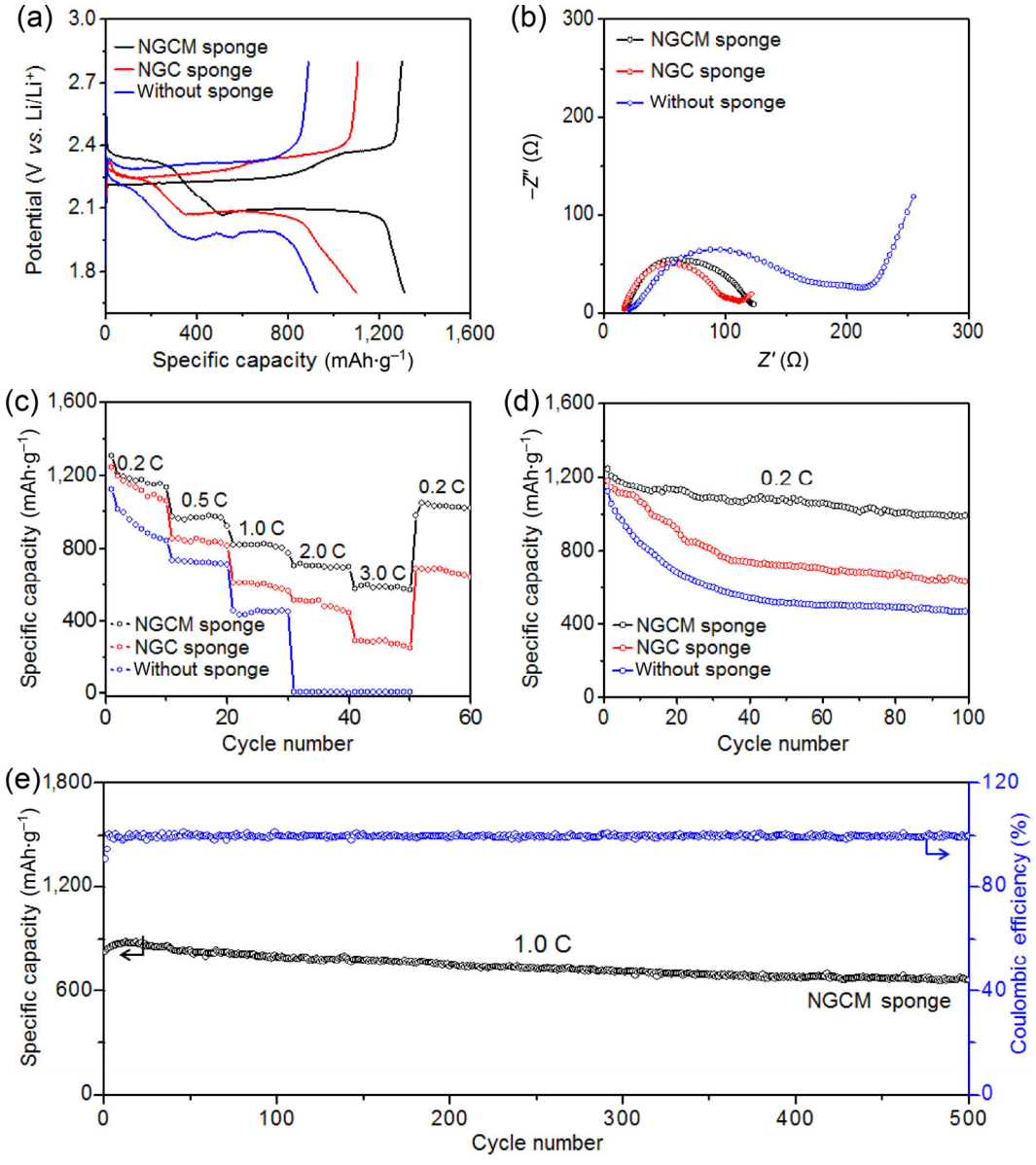

Figure 4 Electrochemical performances of S/CNTs cathode-based Li-S batteries assembled with or without spongy frameworks. (a) Galvanostatic discharge/charge profiles, (b) Nyquist plots, (c) rate performances, and (d) cycling performances at 0.2 C of S/CNTs cathode-based Li-S cells assembled with NGCM sponge, NGC sponge, and without sponge. (e) Long-term cycling stability and Coulombic efficiencies at 1.0 C of S/CNTs cathode-based Li-S cells assembled with NGCM sponge.

NGCM sponge on the redox kinetics of polysulfides [46, 47].

The resistance characteristics of the Li-S cells were examined by EIS. As shown in Fig. 4(b), the EIS plots mainly consist of semicircles, which represent the charge-transfer resistance of Li-S cells. Clearly, the Li-S cells with NGCM and NGC spongy frameworks exhibit smaller semicircles than the cell without spongy framework, indicating a reduced charge-transfer resistance of the NGCM-based cells. Moreover, the Li-S cells with NGCM spongy framework also exhibit the best rate capability (Fig. 4(c)), delivering high discharge capacities of 1,207, 962, 807, 692, and 593 mAh·g^{-1} at 0.2, 0.5, 1.0, 2.0, and 3.0 C, respectively. In contrast, for the cells assembled with the NGC sponge and without spongy framework, the discharge capacities at 3.0 C are only 284 and 10 mAh·g^{-1}, respectively. The enhancement of the rate performance should be

ascribed to the high electrical conductivity of the NGCM spongy framework and the strong polysulfide retention capability of the MnO_2 nanoflakes.

The cycling stability of the Li-S cells, as a key parameter, was carefully compared. When cycled at 0.2 C, the Li-S cells assembled with the NGCM sponge show an initial discharge capacity of 1,248 mAh·g^{-1}, which gradually decreases to 992 mAh·g^{-1} after 100 cycles, corresponding to a capacity retention of 79.5% (Fig. 4(d)). On the other hand, the Li-S cells with NGC sponge and without sponge show comparable initial discharge capacities of 1,184 and 1,123 mAh·g^{-1}, respectively, which decrease dramatically to 634 and 470 mAh·g^{-1} after 100 cycles, corresponding to capacity retentions of 53.5% and 41.9%, respectively. Moreover, to better illustrate the efficient utilization of sulfur, lithium-ion batteries (LIBs) with CNTs cathode (without loading of active sulfur) and NCGM sponge layer were tested within 1.7–2.8 V vs. Li/Li$^+$ (Fig. S8 in the ESM). The analysis reveals very low discharge capacities (< 40 mAh·g^{-1}), confirming that the CNTs host and the NGCM sponge contribute very little to the total capacities of Li-S batteries. At 1.0 C, the discharge capacity of Li-S cells assembled with the NGCM sponge decreases from 829 to 661 mAh·g^{-1} after 500 cycles, with a capacity retention of 79.7%. Moreover, a Coulombic efficiency close to 100% is still achieved, indicating the suppression of polysulfide shuttle effects (Fig. 4(e)).

The self-discharge rate is another important indicator of the polysulfide shuttling level in Li-S batteries. Figures 5(a)–5(c) show the cycling performances of as-prepared Li-S cells at 0.2 C, with a resting time of 24 h after the 5th charge process. After resting for 24 h, the Li-S cells with the NGCM sponge exhibit a self-discharge ratio (i.e., capacity loss) of 5.4%, which is much lower than those of the cells with NGC sponge (8.3%) or without spongy framework (17.0%) (Figs. 5(d)–5(f)). This result suggests that the NGCM spongy framework can effectively suppress the polysulfide shuttle effect and alleviate the self-discharge issues of Li-S batteries.

The structural integrity and surface states of the NGCM spongy framework after long-term cycling were also investigated. The SEM image of the NGCM sponge shows no obvious morphology changes after 500 cycles at 1.0 C (Fig. 6(a)). The corresponding elemental mappings reveal the presence of Ni, C, Mn,

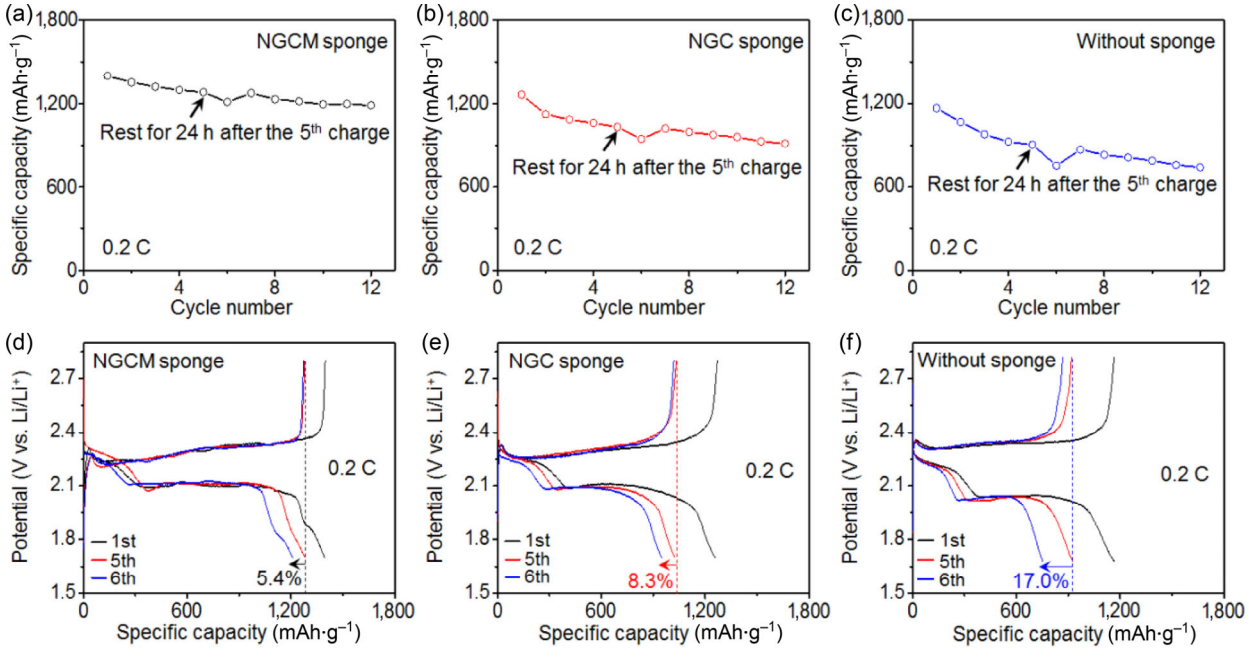

Figure 5 Mitigation of self-discharge enabled by NGCM spongy framework. (a)–(c) Capacity retention and (d)–(f) corresponding galvanostatic discharge/charge profiles at 0.2 C of Li-S cells with (a) and (d) NGCM sponge, (b) and (e) NGC sponge, and (c) and (f) without sponge. The Li-S cells were rested for 24 h between the 5th and 6th discharge steps.

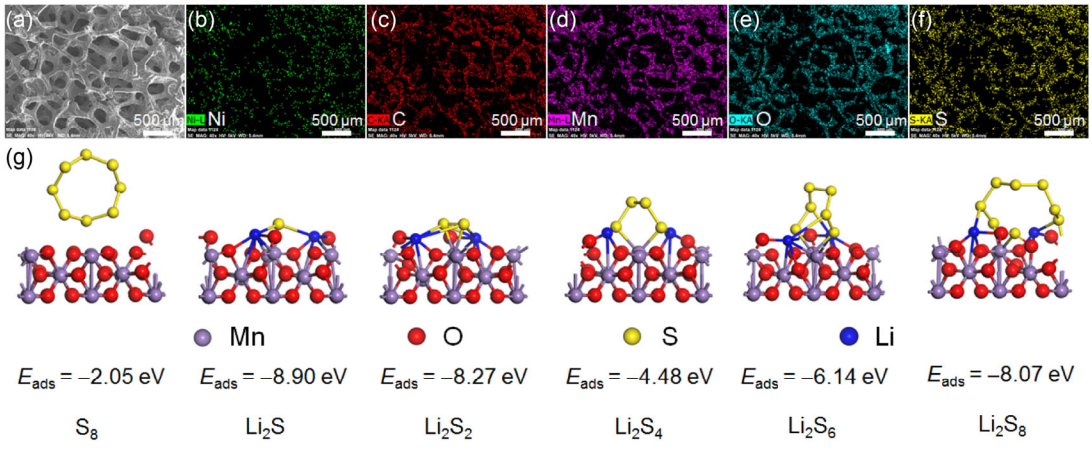

Figure 6 Characterizations of NGCM spongy framework after long-term cycling and calculation of chemisorption capability of MnO_2 for sulfur species. (a) SEM image and (b)–(f) corresponding elemental mappings. (g) DFT-calculated possible structural geometries and binding energies between the (001) planes of MnO_2 and adsorbed sulfur species.

O, and S elements (Figs. 6(b)–6(f)), corresponding to the polysulfides adsorbed on the surface, which provides direct evidence for the polysulfide reservoir ability of the NGCM sponge.

The chemical binding between MnO_2 nanoflakes and sulfur species was simulated by the DFT method (Fig. 6(g)). The most exposed and stable (001) plane of MnO_2 was selected as the absorption interface for calculating its chemisorption ability for sulfur species. The binding energies of MnO_2 (001) planes with S_8, Li_2S, Li_2S_2, Li_2S_4, Li_2S_6, and Li_2S_8 species were calculated to be –2.05, –8.90, –8.27, –4.48, –6.14, and –8.07 eV, respectively. These binding energies are much higher than those between graphitic carbon and sulfur species [40], indicating the strong polysulfide chemisorption and retention capability of the NGCM spongy framework. Adsorption tests were conducted to further confirm the strong chemisorption ability of the NGCM spongy framework. As shown in Fig. S9 in the ESM, after adding the NGCM and NGC spongy frameworks to 0.002 M Li_2S_4 in DME/DOL (1:1 in volume), the solution with the NGCM spongy framework turns almost colorless within 24 h, while the solution with the NGC spongy framework remains yellow.

4 Conclusions

In summary, in this work we propose the design of a 3D spongy framework serving as a polysulfide reservoir layer in Li-S batteries. Benefitting from the hierarchical porous structure, high conductivity, superlyophilic properties, as well as the strong chemisorptive and electrocatalytic effects with polysulfides of the NGCM sponge, Li-S cells assembled with it can efficiently suppress the shuttle effect of polysulfides, exhibiting improved specific capacity, rate capability, cycling stability, and reduced self-discharge rate.

Acknowledgements

This work is supported by the National Key R&D Program of China (Nos. 2017YFA0208200, 2016YFB0700600, and 2015CB659300), the National Natural Science Foundation of China (Nos. 21403105, 21573108, and 51761135104), Natural Science Foundation of Jiangsu Province (Nos. BK20150583 and BK20170644), and the Fundamental Research Funds for the Central Universities (No. 020514380107).

Electronic Supplementary Material: Supplementary material (Figs. S1–S9) is available in the online version of this article at https://doi.org/10.1007/s12274-018-2168-8.

References

[1] Ji, X. L.; Lee, K. T.; Nazar, L. F. A highly ordered nanostructured carbon–sulphur cathode for lithium–sulphur

batteries. *Nat. Mater.* **2009**, *8*, 500–506.

[2] Wang, H. L.; Yang, Y.; Liang, Y. Y.; Robinson, J. T.; Li, Y. G.; Jackson, A.; Cui, Y.; Dai, H. J. Graphene-wrapped sulfur particles as a rechargeable lithium–sulfur battery cathode material with high capacity and cycling stability. *Nano Lett.* **2011**, *11*, 2644–2647.

[3] Manthiram, A.; Fu, Y. Z.; Chung, S. H.; Zu, C. X.; Su, Y. S. Rechargeable lithium–sulfur batteries. *Chem. Rev.* **2014**, *114*, 11751–11787.

[4] Yang, Y.; Zheng, G. Y.; Cui, Y. Nanostructured sulfur cathodes. *Chem. Soc. Rev.* **2013**, *42*, 3018–3032.

[5] Jayaprakash, N.; Shen, J.; Moganty, S. S.; Corona, A.; Archer, L. A. Porous hollow carbon@sulfur composites for high-power lithium-sulfur batteries. *Angew. Chem., Int. Ed.* **2011**, *50*, 5904–5908.

[6] Schuster, J.; He, G.; Mandlmeier, B.; Yim, T.; Lee, K. T.; Bein, T.; Nazar, L. F. Spherical ordered mesoporous carbon nanoparticles with high porosity for lithium–sulfur batteries. *Angew. Chem., Int. Ed.* **2012**, *51*, 3591–3595.

[7] Manthiram, A.; Fu, Y. Z.; Su, Y. S. Challenges and prospects of lithium–sulfur batteries. *Acc. Chem. Res.* **2013**, *46*, 1125–1134.

[8] Yin, Y. X.; Xin, S.; Guo, Y. G.; Wan, L. J. Lithium–sulfur batteries: Electrochemistry, materials, and prospects. *Angew. Chem., Int. Ed.* **2013**, *52*, 13186–13200.

[9] Elazari, R.; Salitra, G.; Garsuch, A.; Panchenko, A.; Aurbach, D. Sulfur-impregnated activated carbon fiber cloth as a binder-free cathode for rechargeable Li-S batteries. *Adv. Mater.* **2011**, *23*, 5641–5644.

[10] Seh, Z. W.; Wang, H. T.; Hsu, P. C.; Zhang, Q. F.; Li, W. Y.; Zheng, G. Y.; Yao, H. B.; Cui, Y. Facile synthesis of Li_2S-polypyrrole composite structures for high-performance Li_2S cathodes. *Energy Environ. Sci.* **2014**, *7*, 672–676.

[11] Li, Z.; Jiang, Y.; Yuan, L. X.; Yi, Z. Q.; Wu, C.; Liu, Y.; Strasser, P.; Huang, Y. H. A highly ordered meso@microporous carbon-supported sulfur@smaller sulfur core–shell structured cathode for Li-S batteries. *ACS Nano* **2014**, *8*, 9295–9303.

[12] Wang, Y. K.; Zhang, R. F.; Pang, Y. C.; Chen, X.; Lang, J. X.; Xu, J. J.; Xiao, C. H.; Li, H. L.; Xi, K.; Ding, S. J. Carbon@ titanium nitride dual shell nanospheres as multi-functional hosts for lithium sulfur batteries. *Energy Storage Mater.* **2019**, *16*, 228−235.

[13] Miao, L. X.; Wang, W. K.; Yuan, K. G.; Yang, Y. S.; Wang, A. B. A lithium–sulfur cathode with high sulfur loading and high capacity per area: A binder-free carbon fiber cloth–sulfur material. *Chem. Commun.* **2014**, *50*, 13231–13234.

[14] Zhao, M. Q.; Liu, X. F.; Zhang, Q.; Tian, G. L.; Huang, J. Q.; Zhu, W. C.; Wei, F. Graphene/single-walled carbon nanotube hybrids: One-step catalytic growth and applications for high-rate Li–S batteries. *ACS Nano* **2012**, *6*, 10759–10769.

[15] Yuan, L. X.; Yuan, H. P.; Qiu, X. P.; Chen, L. Q.; Zhu, W. T. Improvement of cycle property of sulfur-coated multi-walled carbon nanotubes composite cathode for lithium/sulfur batteries. *J. Power Sources* **2009**, *189*, 1141–1146.

[16] Song, J. X.; Xu, T.; Gordin, M. L.; Zhu, P. Y.; Lv, D. P.; Jiang, Y. B.; Chen, Y. S.; Duan, Y. H.; Wang, D. H. Nitrogen-doped mesoporous carbon promoted chemical adsorption of sulfur and fabrication of high-areal-capacity sulfur cathode with exceptional cycling stability for lithium-sulfur batteries. *Adv. Funct. Mater.* **2014**, *24*, 1243–1250.

[17] Lee, J. T.; Zhao, Y. Y.; Thieme, S.; Kim, H.; Oschatz, M.; Borchardt, L.; Magasinski, A.; Cho, W. I.; Kaskel, S.; Yushin, G. Sulfur-infiltrated micro- and mesoporous silicon carbide-derived carbon cathode for high-performance lithium sulfur batteries. *Adv. Mater.* **2013**, *25*, 4573–4579.

[18] Zheng, G. Y.; Zhang, Q. F.; Cha, J. J.; Yang, Y.; Li, W. Y.; Seh, Z. W.; Cui, Y. Amphiphilic surface modification of hollow carbon nanofibers for improved cycle life of lithium sulfur batteries. *Nano Lett.* **2013**, *13*, 1265–1270.

[19] Yuan, Z.; Peng, H. J.; Hou, T. Z.; Huang, J. Q.; Chen, C. M.; Wang, D. W.; Cheng, X. B.; Wei, F.; Zhang, Q. Powering lithium-sulfur battery performance by propelling polysulfide redox at sulfiphilic hosts. *Nano Lett.* **2016**, *16*, 519–527.

[20] Yu, M. P.; Ma, J. S.; Song, H. Q.; Wang, A. J.; Tian, F. Y.; Wang, Y. S.; Qiu, H.; Wang, R. M. Atomic layer deposited TiO_2 on a nitrogen-doped graphene/sulfur electrode for high performance lithium-sulfur batteries. *Energy Environ. Sci.* **2016**, *9*, 1495–1503.

[21] Li, Z.; Zhang, J. T.; Lou, X. W. Hollow carbon nanofibers filled with MnO_2 nanosheets as efficient sulfur hosts for lithium–sulfur batteries. *Angew. Chem., Int. Ed.* **2015**, *54*, 12886–12890.

[22] Tao, X. Y.; Wang, J. G.; Liu, C.; Wang, H. T.; Yao, H. B.; Zheng, G. Y.; Seh, Z. W.; Cai, Q. X.; Li, W. Y.; Zhou, G. M.; Zu, C. X.; Cui, Y. Balancing surface adsorption and diffusion of lithium-polysulfides on nonconductive oxides for lithium-sulfur battery design. *Nat. Commun.* **2016**, *7*, 11203.

[23] Li, Z. Q.; Li, C. X.; Ge, X. L.; Ma, J. Y.; Zhang, Z. W.; Li, Q.; Wang, C. X.; Yin, L. W. Reduced graphene oxide wrapped MOFs-derived cobalt-doped porous carbon polyhedrons as sulfur immobilizers as cathodes for high performance lithium sulfur batteries. *Nano Energy* **2016**, *23*, 15–26.

[24] Li, Y. J.; Fan, J. M.; Zheng, M. S.; Dong, Q. F. A novel synergistic composite with multi-functional effects for high-performance Li-S batteries. *Energy. Environ. Sci.* **2016**, *9*, 1998–2004.

[25] Lin, Z.; Liu, Z. C.; Fu, W. J.; Dudney, N. J.; Liang, C. D. Lithium polysulfidophosphates: A family of lithium-conducting sulfur-rich compounds for lithium-sulfur batteries. *Angew. Chem., Ed. Int.* **2013**, *125*, 7608−7611.

[26] Lin, Z.; Liu, Z. C.; Fu, W. J.; Dudney, N. J.; Liang, C. D. Phosphorous pentasulfide as a novel additive for high-performance lithium-sulfur batteries. *Adv. Funct. Mater.* **2013**, *23*, 1064–1069.

[27] Huang, C.; Xiao, J.; Shao, Y. Y.; Zheng, J. M.; Bennett, W. D.; Lu, D. P.; Saraf, L. V.; Engelhard, M.; Ji, L. W.; Zhang, J. G.; Li, X. L.; Graff, G. L.; Liu, J. Manipulating surface reactions in lithium-sulphur batteries using hybrid anode structures. *Nat. Commun.* **2014**, *5*, 3343.

[28] Zhang, Y. J.; Liu X. Y.; Bai, W. Q.; Tang, H.; Shi, S. J.; Wang, X. L.; Gu, C. D.; Tu, J. P. Magnetron sputtering amorphous carbon coatings on metallic lithium: Towards promising anodes for lithium secondary batteries. *J. Power Sources* **2014**, *266*, 43–50.

[29] Kim, J. S.; Kim D. W.; Jung, H. T.; Choi, J. W. Controlled lithium dendrite growth by a synergistic effect of multilayered graphene coating and an electrolyte additive. *Chem. Mater.* **2015**, *27*, 2780–2787.

[30] Tang, C.; Zhang, Q.; Zhao, M. Q.; Huang, J. Q.; Cheng, X. B.; Tian, G. L.; Peng, H. J.; Wei, F. Nitrogen-doped aligned carbon nanotube/graphene sandwiches: Facile catalytic growth on bifunctional natural catalysts and their applications as scaffolds for high-rate lithium-sulfur batteries. *Adv. Mater.* **2014**, *26*, 6100−6105.

[31] Zhao, M. Q.; Zhang, Q.; Huang, J. Q.; Tian, G. L.; Nie, J. Q.; Peng, H. J.; Wei, F. Unstacked double-layer templated graphene for high-rate lithium-sulphur batteries. *Nat. Commun.* **2014**, *5*, 3410.

[32] Kim, A. Y.; Kim, M. K.; Kim, J. Y.; Wen, Y. R.; Gu, L.; Dao, V. D.; Choi, H. S.; Byun, D.; Lee, J. K. Ordered SnO nanoparticles in MWCNT as a functional host material for high-rate lithium-sulfur battery cathode. *Nano Res.* **2017**, *10*, 2083−2095.

[33] Dong, X. C.; Ma, Y. W.; Zhu, G. Y.; Huang, Y. X.; Wang, J.; Chan-Park, M. B.; Wang, L. H.; Huang, W.; Chen, P. Synthesis of graphene-carbon nanotube hybrid foam and its use as a novel three-dimensional electrode for electrochemical sensing. *J. Mater. Chem.* **2012**, *22*, 17044–17048.

[34] Graf, D.; Molitor, F.; Ensslin, K.; Stampfer, C.; Jungen, A.; Hierold, C.; Wirtz, L. Spatially resolved Raman spectroscopy of single-and few-layer graphene. *Nano Lett.* **2007**, *7*, 238–242.

[35] Liu, J. P.; Jiang, J.; Cheng, C. W.; Li, H. X.; Zhang, J. X.; Gong, H.; Fan, H. J. Co_3O_4 nanowire@MnO_2 ultrathin nanosheet core/shell arrays: A new class of high-performance pseudocapacitive materials. *Adv. Mater.* **2011**, *23*, 2076–2081.

[36] Chen, S.; Zhu, J. W.; Wu, X. D.; Han, Q. F.; Wang, X. Graphene oxide-MnO_2 nanocomposites for supercapacitors. *ACS Nano* **2010**, *4*, 2822–2830.

[37] Yan, J.; Fan, Z. J.; Wei, T.; Cheng, J.; Shao, B.; Wang, K.; Song, L. P.; Zhang, M. L. Carbon nanotube/MnO_2 composites synthesized by microwave-assisted method for supercapacitors with high power and energy densities. *J. Power Sources* **2009**, *194*, 1202–1207.

[38] Xiao, Z. B.; Yang, Z.; Wang, L.; Nie, H. G.; Zhong, M. E.; Lai, Q. Q.; Xu, X. J.; Zhang, L. J.; Huang, S. M. A lightweight TiO_2/graphene interlayer, applied as a highly effective polysulfide absorbent for fast, long-life lithium-sulfur batteries. *Adv. Mater.* **2015**, *27*, 2891–2898.

[39] Hu, G. J.; Sun, Z. H.; Shi, C.; Fang, R. P.; Chen, J.; Hou, P. X.; Liu, C.; Cheng, H. M.; Li, F. A sulfur-rich copolymer@CNT hybrid cathode with dual-confinement of polysulfides for high-performance lithium-sulfur batteries. *Adv. Mater.* **2017**, *29*, 1603835.

[40] Ma, L. B.; Yuan, H.; Zhang, W. J.; Zhu, G. Y.; Wang, Y. R.; Hu, Y.; Zhao, P. Y.; Chen, R. P.; Chen, T.; Liu, J.; Hu, Z.; Jin, Z. Porous-shell vanadium nitride nanobubbles with ultrahigh areal sulfur loading for high-capacity and long-life lithium-sulfur batteries. *Nano Lett.* **2017**, *17*, 7839–7846.

[41] Yuan, Z.; Peng, H. J.; Hou, T. Z.; Huang, J. Q.; Chen, C. M.; Wang, D. W.; Cheng, X. B.; Wei, F.; Zhang, Q. Powering lithium-sulfur battery performance by propelling polysulfide redox at sulfiphilic hosts. *Nano Lett.* **2016**, *16*, 519−527.

[42] Pang, Q.; Kundu, D.; Cuisinier, M.; Nazar, L. F. Surface-enhanced redox chemistry of polysulphides on a metallic and polar host for lithium-sulphur batteries. *Nat. Commun.* **2014**, *5*, 4759.

[43] Zhao, Y.; Wu, W. L.; Li, J. X.; Xu, Z. C.; Guan, L. H. Encapsulating MWNTs into hollow porous carbon nanotubes: A tube-in-tube carbon nanostructure for high-performance lithium-sulfur batteries. *Adv. Mater.* **2014**, *26*, 5113–5118.

[44] Lee, J. S.; Kim, W.; Jang, J.; Manthiram, A. Sulfur-embedded activated multichannel carbon nanofiber composites for long-life, high-rate lithium-sulfur batteries. *Adv. Energy Mater.* **2016**, *7*, 1601943.

[45] Jin, F. Y.; Xiao, S.; Lu, L. J.; Wang, Y. Efficient activation of high-loading sulfur by small CNTs confined inside a large CNT for high-capacity and high-rate lithium-sulfur batteries. *Nano Lett.* **2016**, *16*, 440–447.

[46] Ma, L. B.; Chen, R. P.; Zhu, G. Y.; Hu, Y.; Wang, Y. R.; Chen, T.; Liu, J.; Jin, Z. Cerium oxide nanocrystal embedded bimodal micromesoporous nitrogen-rich carbon nanospheres as effective sulfur host for lithium-sulfur batteries. *ACS Nano* **2017**, *11*, 7274–7283.

[47] Zhou, G. M.; Tian, H. Z.; Jin, Y.; Tao, X. Y.; Liu, B. F.; Zhang, R. F.; Seh, Z. W.; Zhuo, D.; Liu, Y. Y.; Sun, J.; Zhao, J.; Zu, C. X.; Wu, D. S.; Zhang, Q. F.; Cui, Y. Catalytic oxidation of Li_2S on the surface of metal sulfides for Li-S batteries. *Proc. Natl. Acad. Sci. USA* **2017**, *114*, 840−845.